HPC Predictions of Primary Atomization with SPH: Validation and Comparison to Experimental Results

Samuel Braun, Simon Holz, Lars Wieth, Thilo F. Dauch, Marc C. Keller, Geoffroy Chaussonnet,
Corina Schwitzke, Rainer Koch, Hans-Jörg Bauer
Institut für Thermische Strömungsmaschinen
Karlsruhe Institute of Technology
Karlsruhe, Germany
samuel.braun@kit.edu

***Abstract*—The prediction of atomization is associated to extremely high numerical costs and requires a very accurate modeling of the involved physical processes. State of the art Eulerian multi-phase simulation methods failed to reliably predict the spray characteristics of air-assisted atomizers. In this paper we qualitatively and quantitatively evaluate the capabilities of the SPH method with respect to its applicability to this multiscale phenomenon. By means of 2D simulations of a generic airblast atomizer, we compare the SPH spray predictions with the results obtained by commonly used Eulerian multiphase methods. Furthermore, the convergence behavior of SPH has been investigated by varying the spatial resolution by a factor of 20. The convergence criterion is the appearance of droplets consisting of a single particle. It can be shown, that the convergence rate follows a power law. A 3D simulation consisting of 1.2 billion particles is compared to the results from experimental investigations. The simulation is capable to phenomenologically predict the experimentally observed breakup mechanisms. Knowing, that the small number of simulated breakup events does not allow any statistically significant statement, we observe, that the numerically predicted characteristic and mean fuel droplet sizes coincide with the experimentally measured droplet sizes.**

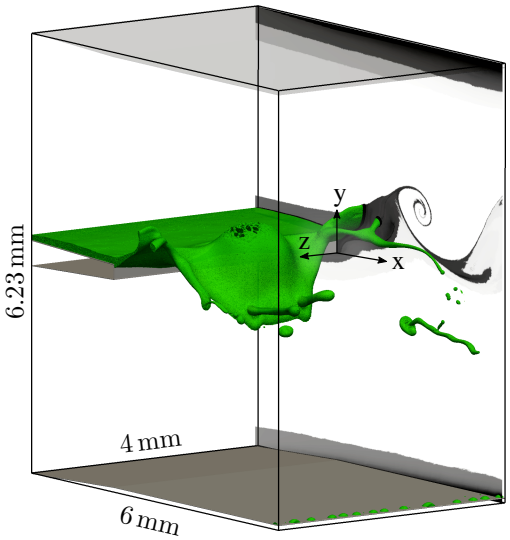

Fig. 1: 3D computational domain of the planar prefilming airblast atomizer.

I. Introduction

A well defined positioning of liquid fuel inside the combustion chamber determines the location of the flame and, therefore, allows to minimize the toxic emissions of aircraft engines. However, due to the enormous computational costs associated to the simulation of the breakup process of air-assisted nozzles, state of the art Eulerian multi-phase simulation methods failed to reliably predict the fuel spray characteristics. In contrast to the atomization of liquid jets, which is widely investigated experimentally as well a numerically, the underlying physical effects of air-assisted atomization are not understood in detail. The numerical effort for the simulations results from the following properties of primary breakup: The scales to be considered cover at least 4 orders of magnitude in time and space. Concerning the discretization, this results in many discretization points and small time steps. Atomization strictly requires a three-dimensional, transient consideration. The influence of turbulent fluctuations of the gaseous phase on primary atomization is not known. Therefore, the modeling of turbulence is not appropriate and a Direct Numerical Simulation (DNS) is required. From a numerical point of view, the large density ratios between the gaseous phase and the liquid to be atomized can cause stability issues. Whereas above mentioned features also apply for pressure atomizers, air-assisted atomization is additionally characterized by the fact, that the mean velocity of the liquid phase is typically two orders of magnitude lower than the velocity of the atomizing air stream. Therefore, the simulation has to cover a rather long period of physical time.

With regard to multi-phase flows, SPH offers a superior simulation capability. This concerns both, the physical correctness of the predictions as well as the computational performance. Recent attempts to numerically predict air-assisted atomization using the Finite Volume approach in combination with the Volume of Fluid (VoF) method [14], [15] already provide valuable insights into the flow physics. However, the predicted droplet sizes strongly depend on the choice of the volume fraction, which is used to distinguish between the gaseous and the liquid phase. Furthermore, the raw computational performance is about one order of magnitude below our SPH code presented in [2], [3]. In this paper we demonstrate, that large-scale 3D SPH simulations are capable to precisely

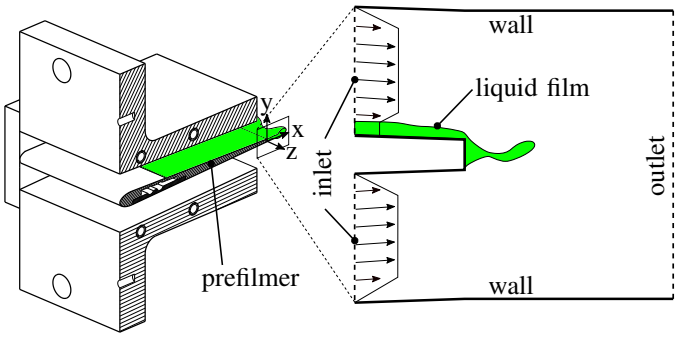

Fig. 2: Experimental setup of the planar prefilming airblast atomizer (left) and its numerical abstraction.

predict primary atomization. Therefore, the simulation already presented in [2] is re-evaluated and qualitatively and quantitatively compared to the experimental reference investigation. Due to the Lagrangian nature of the method, interface diffusion and deficient mass conservation are inherently avoided. Thanks to the outstanding serial and parallel performance, the required numerical resources are comparatively slow.

The structure of the paper is as follows. In section II we briefly recall the experimental reference investigation and describe the corresponding computational domain and the physical models used in the following investigations. In section III we describe the main post-processing steps for both, experiment and simulation. In section IV the results of the numerical investigations are presented. Section IV-A allows to estimate the capabilities of SPH in comparison to Volume of Fluid simulations. In section IV-B, the convergence behavior of SPH is examined with respect to the representation of small droplets. In section IV-C, the qualitative and quantitative results from the 3D simulation are opposed to the experimental reference data. Section V helps to classify the achieved computational performance in comparison to state of the art Level Set or Volume of Fluid methods. In section VI the results are summarized.

II. Experimental and numerical setup

A. Experimental test section

The main part of the experimental reference test section consists of an airfoil shaped planar structure, which mimics an uncoiled section of a real annular atomizer. This so called prefilmer is exposed to the atomizing air flow. On the upper side of the prefilmer, a fuel film is applied. Due to the aerodynamic forces, the film is pushed towards the trailing edge of the prefilmer. Depending on the surface tension and the flow configuration, a liquid bulge develops. This liquid reservoir is excited by the fluctuating aerodynamic forces and finally detaches from the trailing edge. The detachment and disintegration into small droplets is called primary atomization. Figure 2 (left) illustrates the main part of the experimental test section. The fuel is depicted in green. The atomization behavior is mainly performed using High Speed Shadowgraphy. The area of interest is the x-z-plane, downstream the trailing edge. The experimental investigations are described in [5]–[7].

B. Numerical model

The numerical domain covers the region in vicinity of the trailing edge. It is confined by a static upper and lower wall and by inlet and outlet boundary conditions. In case of the 3D simulation, the 2D section is extruded in z-direction, and the lateral faces are confined by translational periodic boundary conditions. The exact dimensions, the operating point and the fluid properties are listed in [2]. An overview of the 2D and 3D computational domains is given in Figs. 1 and 2.

The 2D domain is used for the cross-comparison to grid-based simulation methods and for the convergence study. The 3D domain is devoted to the comparison to the experiment. The spatial discretization of the SPH and VoF simulations is $5\,\mu\mathrm{m}$. The 2D domains consist of 1.5 million particles respectively grid cells. The 3D domain consists of more than 1.2 billion particles. For the convergence study, the inter-particle spacing dx has been varied between $20\,\mu\mathrm{m}$ and $1\,\mu\mathrm{m}$. The applied physical models are the density equation as proposed by Hu and Adams [9], in order to handle the interfacial discontinuities. Wall wetting effects and surface tension are taken into account using the models proposed by Adami et al. [1] and Wieth et al. [16]. We apply a quintic spline kernel with $h = 1.0 \cdot dx$ or a Wendland kernel with $h = 1.3 \cdot dx$. A detailed performance analysis of the parallel code basis `super_sph` is given in [10].

III. Diagnostics and post-processing

A. High speed shadowgraphy

The data acquisition for the experimental investigations performed by Gepperth et al. [6] is based on various laser-optical methods and high speed imaging. In this work we mainly utilize a simplified version of the Particle Tracking Velocimetry developed by Gepperth et al. [7], which allows to characterize the liquid phase. The raw data acquisition uses backlight illumination of the measurement volume with a double-pulsed laser in combination with a coupled high speed CCD camera. The image processing consists of identifying the connected structures. A modified Particle Image Velocimetry (PIV) method is used in order to derive the ligament deformation rates and droplet speeds. The droplet sizes have been corrected using a calibration plate. The detected ligaments and droplets are approximated by ellipsoids so as to derive their mass and a representative diameter. The smallest quantifiable droplets have a diameter of $30\,\mu\mathrm{m}$. In contrast to Gepperth et al. [7] we do not apply a depth-of-field correction to the measured droplet sizes. Therefore, the measuring uncertainty of less than $4\,\%$ must be considered to be higher.

B. Ligament and droplet detection

In order to detect droplets, connected clusters of particles representing the liquid phase have to be identified. Therefore, a Connected Component Labeling (CCL) [12] technique is

applied. As a result, every detected cluster has a unique ID and can be further classified by e.g. a deformation index, center of gravity, mass or velocity. More details on this post-processing step can be found in [2].

C. Spray characterization

The quantitative classification of sprays is based on characteristic or mean droplet diameters. The characteristic mass median diameter $D_{V0.5}$ represents the maximum diameter of droplets (arranged in order of ascending mass) which make up $50\,\%$ of the atomized liquid mass. Accordingly, $10\,\%$ of the atomized mass is bound in droplets smaller than $D_{V0.1}$. The Sauter Mean Diameter (D_{32}) is a measure for the volume to surface ratio of the entirety of droplets of a spray. An ideal mono-disperse spray and a real spray have the same volume to surface ratio, if their D_{32} is equal.

D. Quantitative comparison

The comparison of spray characteristics obtained with the graphical workflow (experiment) and the CCL-based post-processing (SPH) has been limited to quasi spherical droplets, with a maximum aspect ratio of 2. At larger deformation rates, the elliptical approximation and, therefore, the estimate of the corresponding droplet diameter, would lead to erroneous results. A direct cross-comparison to the graphical method has been performed using a highly resolved image from the simulation result. Minor deviations from the exact CCL-solution mainly result from the superposition of (large) droplets.

IV. Results on atomization prediction

A. Comparison to Volume of Fluid simulations

In this section we investigate the atomization behavior of SPH be means of 2D simulations. As mentioned earlier, primary breakup strictly requires a 3D, transient treatment. Therefore, any comparison of the resulting data to experimentally obtained quantitative features is prohibitive. However, in order to assess the principal qualification of SPH, comparative 2D simulations with commonly used grid-based Finite Volume tools have been performed with identical initial and boundary conditions and equal spatial discretization. This investigation, therefore, is not a validation, but a comparison of "numerics with numerics". The grid-based tools are the standard Volume of Fluent solvers of the CFD toolkits OpenFOAM® 2.3.0 (`interFoam`) and ANSYS® Fluent, Release 15.0.7. In Fig. 3 a typical breakup sequence for each of the investigated tools is depicted. For the VoF simulations, the displayed liquid corresponds to volume fractions greater than 0.2. The time increment between two consecutive images is $\Delta t \approx 150\,\mu s$. The first image of a sequence corresponds to the last (stored) time step just before the burst of the main ligament, which is attached to the prefilmer lip. Looking at the leftmost images, SPH shows a less pronounced stretching and deflection of the main ligament, than the other methods. However, as soon as the large ligament starts to disintegrate, SPH and Fluent show a similar behavior with many small droplets. OpenFOAM

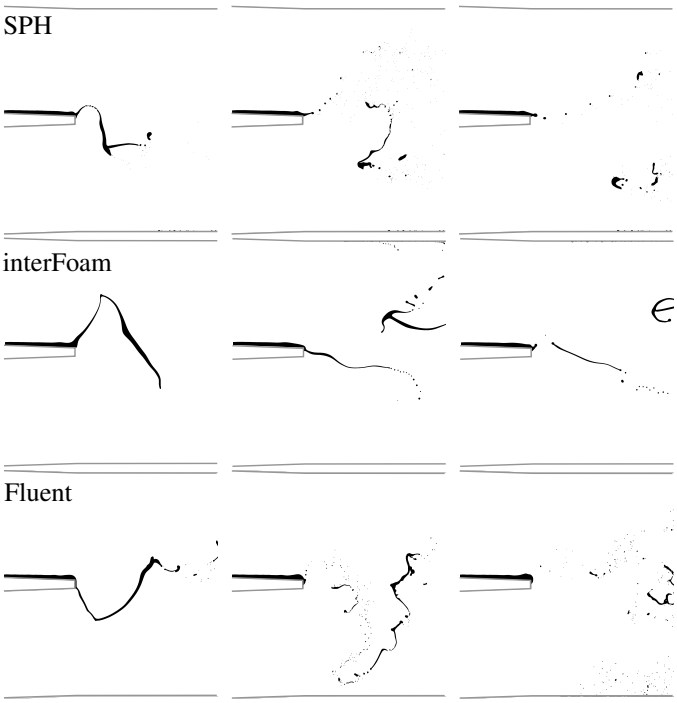

Fig. 3: Breakup sequences obtained with the different simulation tools. The time increment between two consecutive images is $\Delta t \approx 150\,\mu s$.

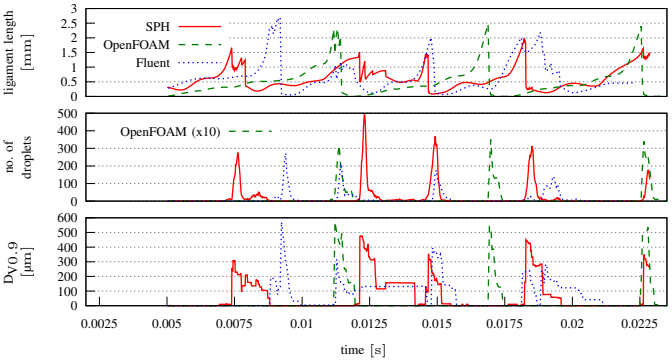

Fig. 4: Derived temporal atomization characteristics: evolution of the ligament length, the number of droplets and the characteristic droplet diameter $D_{V0.9}$.

visibly generates much less droplets and the elongated secondary ligaments seem to be very stable. Fig. 4 quantifies the observations. The length of the main ligament, the number of generated droplets and the mass median diameter $D_{V0.9}$ are plotted over time. Except for the first breakup event, SPH and Fluent predict similar ligament lengths at the moment of the burst. OpenFOAM, in general, predicts higher breakup lengths. The most noticeable difference is visible for the number of generated droplets. Whereas the predictions of SPH and Fluent are of the same order of magnitude, OpenFOAM

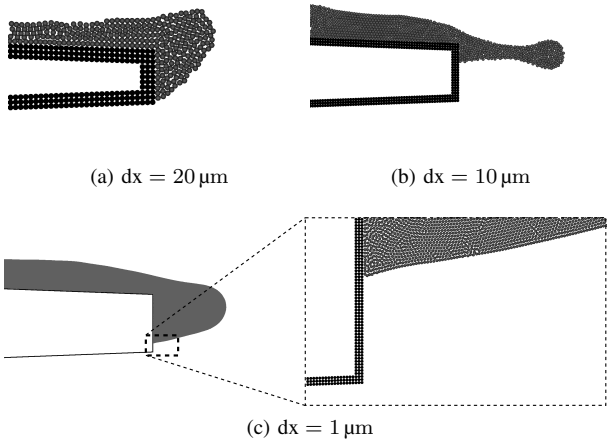

Fig. 5: Illustration of the different levels of discretization. Depiction of the area in vicinity of the prefilmer trailing edge.

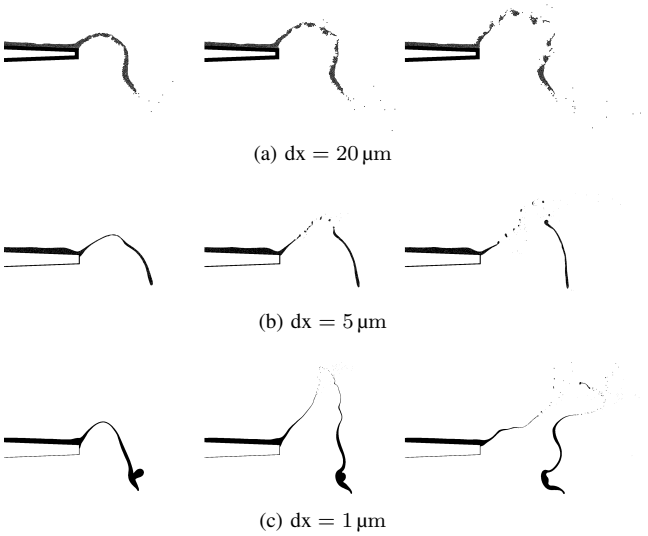

Fig. 6: Representative breakup sequences obtained with different inter-particle spacings dx. The time increment between two consecutive images is $\Delta t \approx 47\,\mu s$.

predicts one order of magnitude less droplets than the other tools. When comparing the breakup frequencies, SPH (279 Hz) and Fluent (288 Hz) also show similar values, in contrast to OpenFOAM (157 Hz). In summary, based on the performed cross-comparison of the different numerical tools, a conclusive estimate on the physical correctness is not possible. However, SPH and Fluent predict comparable atomization features, whereas OpenFOAM produces clearly distinguishable results.

B. Convergence behavior

Typically, the required spatial resolution for a single phase DNS can be estimated by evaluating the Kolmogorov length scale. Disperse multiphase flows with a non-negligible influence of surface tension may feature liquid structures with even smaller length scales. Therefore, a parametric study has been performed in order to quantify the effect of discretization length on the resulting spray characteristics. As convergence criterion, the relative number of droplets consisting of only one single particle has been chosen. A sufficiently small (probably dx $\rightarrow$ 0) discretization length would result in an absence of these single particle droplets (SPD). The computational domain has been discretized by particles with an inter-particle spacing of dx $= \{1, 2.5, 5, 10, 20\}\mu m$. For all discretization levels, an identical set of physical and numerical constants (speed of sound, background pressure) has been used. In contrast to the investigations presented in section in IV-A, a Wendland kernel with $h = 1.3 \cdot$ dx has been applied. This leads in smoother phase interfaces and considerably lower computational costs. In Fig. 5 the two coarsest and the finest discretization levels are illustrated, the walls are depicted by black spheres, the liquid by gray ones. The height of the trailing edge is 230 µm.

In Fig. 6 representative breakup sequences at three different discretization levels are depicted. At the coarsest level, the main ligament virtually undergoes a catastrophic breakup with

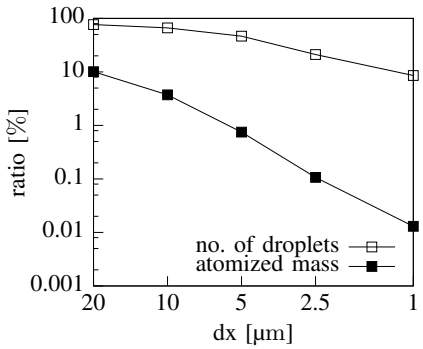

Fig. 7: Convergence behavior for atomization simulations.

an initially very rugged phase interface. The finer discretization levels feature much smoother interfaces. At a resolution of dx $= 1\,\mu m$, very thin and elongated liquid structures can be observed, which disintegrate in a mechanism similar to the Rayleigh breakup. In Tab. I both the computational effort as well as the simulation results for the different levels of discretization are quantified. The number of droplets ranges from 95 000 to nearly 37 million. The time step length varies between 65 ns and 1.4 ns. The simulations have been performed on up to 1000 compute cores of the ForHLR II[1] cluster. Depending on the numeric effort, the simulations have been terminated after reaching a certain number of simulated time steps or due to (multiples of) the admissible wall clock time per compute job. The simulated physical period of time resulting from the mean time step length and the number of calculated time steps varies between 650 ms and 17 ms. Thus, a different amount of main breakup events have been detected

[1]Forschungshochleistungsrechner ForHLR (Phase) II
https://www.top500.org/system/178840

TABLE I: Computing details and droplet statistics of the convergence study.

dx [µm]	no. of particles	mean Δt [ns]	no. of CPU	no. of time steps	no. of stored time steps	duration [h]	no. of droplets	ratio of SPD [%]	atomized mass in SPD [%]
20	95×10^3	65.0	160	10×10^6	40 000	9.5	532 115	76.7	10.079
10	374×10^3	32.5	500	10×10^6	20 000	6.5	315 675	66.4	3.733
5	1.49×10^6	15.9	1000	10×10^6	10 000	9.8	155 556	46.6	0.751
2.5	5.93×10^6	5.6	1000	20×10^6	3000	71.2	18 848	21.1	0.107
1	36.97×10^6	1.4	1000	12.3×10^6	1231	288	26 493	8.6	0.013

for the different discretization levels. At the coarsest levels, about 200 breakup events could be simulated, at the finest level only 3.

Whereas the absolute number of droplets in Tab. I is of minor interest, the relative amount of SPDs is important. At dx $= 20\,\mu$m, almost $77\,\%$ of the generated droplets consist of only one particle. Even at dx $= 5\,\mu$m, roughly half of the droplets are SPDs. However, looking at the liquid mass which is bound in SPDs, the relative amount is below $1\,\%$. It is worth to mention, that for the calculation of the relative mass, which is bound in SPDs, only the atomized mass is taken into account. By also considering the mass of the liquid film which is attached to the prefilmer lip, the relative mass bound in SPDs drops below $1\,‰$ for all levels of discretization. In Fig. 7, the relative number of SPDs and the relative mass bound in SPDs are shown in a log-log plot. The absolute values of the relative mass bound in SPDs as well as the convergence behavior can be considered as excellent. Furthermore, in three dimensional simulations, the relative mass bound in SPDs is very likely to be below the values obtained in this 2D study.

The superior numerical behavior of SPH for the simulation of multiphase flows with strong liquid-gas interaction gets even more apparent, when looking at state of the art Eulerian methods. In [11], an under-resolved Level Set simulation of a liquid jet in crossflow loses up to $40\,\%$ of the liquid mass, before the tip of the jet touches the outlet section. Under-resolved VoF simulations suffer from strong interface diffusion, hampering an exact localization of the phase interface.

Like in the previous chapter (IV-A), an estimate of the physical correctness of SPH and its superiority to other methods is not possible by performing convergence studies. However, Fig. 8 reveals an interesting insight, concerning the treatment of surface tension by different simulation tools. The upper breakup sequence has been obtained with SPH with dx $= 1\,\mu$m. The lower breakup sequence results from the OpenFOAM simulation with dx $= 5\,\mu$m and has already been shown in Fig. 3. There is a striking similarity of the shapes of the liquid ligaments. However, the thickness of the thread-like structures and the volume of the distorted ligaments differ significantly. This behavior might be attributed to the artificial interface compression term (cf. [13]) in the `interFoam`-solver, which has been introduced to reduce the interface diffusion. It seems like this term introduces a scale-independent and, therefore, questionable stability behavior of the phase interface.

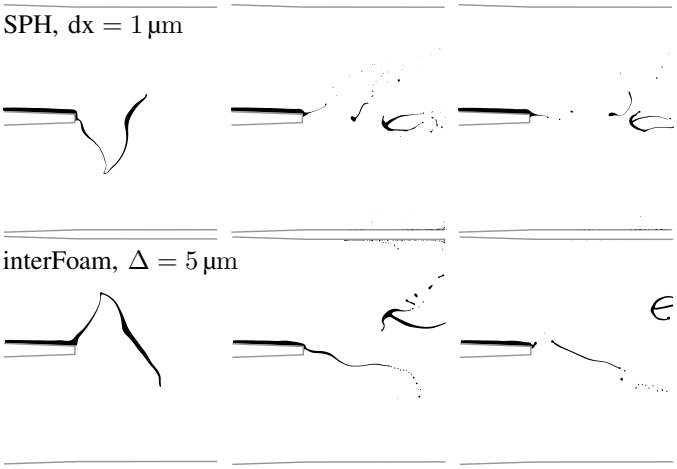

Fig. 8: Comparison of breakup sequences predicted with SPH at dx $= 1\,\mu$m and with `interFoam` at $\Delta = 5\,\mu$m. The time increment between two consecutive images is $\Delta t \approx 150\,\mu$s.

C. Comparison to experimental results

Due to the two-dimensionality, the investigations in sections IV-A and IV-B are not suited to provide any statement concerning the physically correctness when it comes to the simulation of primary atomization. In the following, we re-evaluate the 3D simulation of a section of a planar prefilming airblast atomizer. This simulation has already been presented in [2], however, the quantitative evaluation and the comparison to experimental datasets have not been realized yet. To give a brief summary of the simulation, a few numbers are recalled. The simulation comprises 1.2 billion particles and has been performed on 2560 cores of the ForHLR I[2] cluster. Within 60 days roughly 1.1 million time steps and 14.6 ms of simulated physical time could be achieved. The data size of the 1113 stored time steps is about 69 TB. Due to performance reasons and due to a better phase interface representation, the initially

[2]Forschungshochleistungsrechner ForHLR (Phase) I
https://www.top500.org/system/178424

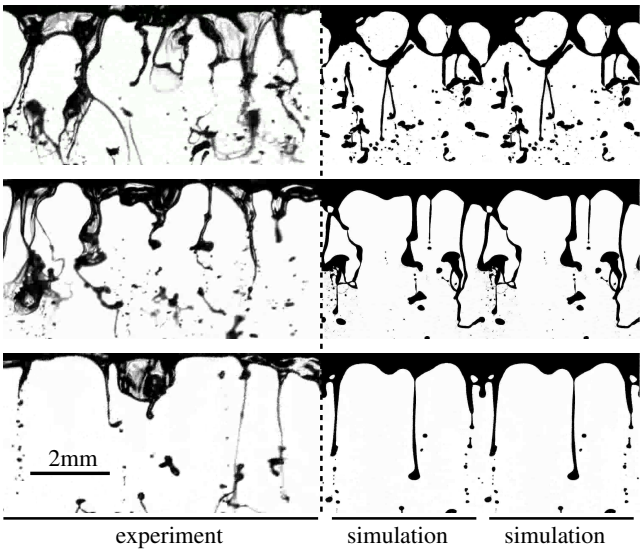

Fig. 9: Top view snapshots of experiment (left half) and simulation. The simulation data is duplicated in span-wise direction. High speed video images: courtesy of S. Gepperth.

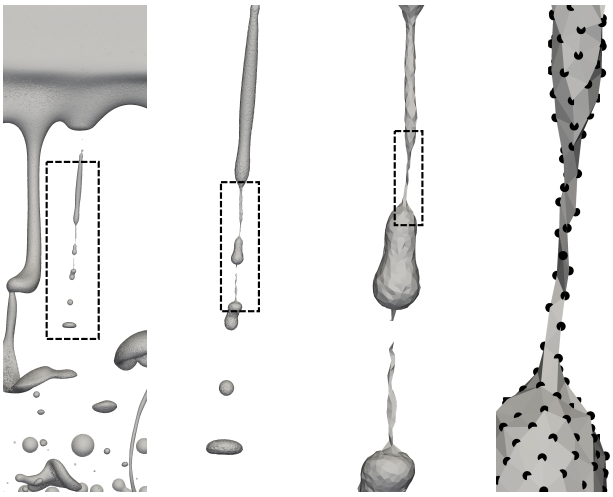

Fig. 10: Close-up of a Rayleigh breakup event. The height of the leftmost image is about $3.8\,\mathrm{mm}$, the height of the rightmost image is about $90\,\mu\mathrm{m}$.

used quintic spline kernel has been replaced by a Wendland kernel after the first third of the simulation period.

1) Qualitative comparison: In Fig. 9 three arbitrary top view (x-z-plane) snapshots of the experimental investigations and the simulation are placed side by side. The size of the displayed experimental section is $8\,\mathrm{mm} \times 4\,\mathrm{mm}$. For descriptive reasons, the simulation data with an extent of only $4\,\mathrm{mm}$ is duplicated in spanwise direction. The simulation features very similar length scales in streamwise and spanwise direction. Also the distortion of the elongated ligaments looks comparable. The furcate shaped structures resulting from a previous bag breakup event are observable in both sets of images. The simulation is able to predict the two major breakup mechanisms, which are known from the experiments: The Rayleigh breakup of elongated thread-shaped ligaments and the bag breakup, which consists of a blow up and burst of larger liquid structures. The bag breakup has already been described in our previous paper [2]. In general, in comparison to the experiments, the liquid bubbles burst too early. The spatial resolution of $5\,\mu\mathrm{m}$ is not sufficient to capture the thin liquid skin of the strongly bloated structures. However, a quantitative comparison of the small droplets resulting from the burst of this skin could not be realized anyway, as their size is below the spatial resolution of the high speed camera. Concerning the formation, the variety of shapes and the disintegration of the thread-like liquid structures, there is no apparent deviation between the experiment and the simulation. It is noteworthy, that the self-organizing property of the SPH particles allows to resolve liquid structures, which are as small as the discretization length scale itself. In Fig. 10 this feature is illustrated for a Rayleigh breakup. At the moment of pinch off, the resulting satellite droplets are connected by a 1D particle chain. A similar self-organizing behavior is also observable for the bag breakup. Here, shortly before the burst, the bloated liquid skin gets as thin as one particle layer. Grid-based methods, in contrast, require at least 3 to 4 grid cells in each direction for the discretization of e.g. a droplet.

2) Quantitative comparison: Within the simulated period of time of $14.6\,\mathrm{ms}$ only two major (bag) breakup events could be detected, after the simulation has reached an fully established 3D flow regime. Therefore, the extraction of statistically irrefutable quantitative spray properties is not possible. Instead, we performed a quantitative single-event analysis. This means, the quantitative statistics of a simulated breakup event have been assessed separately and compared to experimentally observed breakup events. As Fig. 9 indicates, the recognition of clearly identifiable and distinguishable breakup events is difficult. In order to reduce the event density in spanwise direction, we considered a reduced liquid loading of $25\,\mathrm{mm}^2/\mathrm{s}$ instead of $50\,\mathrm{mm}^2/\mathrm{s}$ in case of the experimental operation point. This approach is justified by the results of Gepperth [8], who showed, that the liquid loading does not affect the diameter based spray characteristics at all. In Fig. 11 the two breakup events from the simulation and two breakup events from the experiment are depicted. The time increment between two consecutive sub figures is $300\,\mu\mathrm{s}$ for the simulation (every 20th stored time step) and $143\,\mu\mathrm{s}$ for the experiment (every captured frame). Altogether, 7 experimentally observed breakup events have been subject to the quantitative comparison.

Figure 12 summarizes the quantitative results. For each of the evaluated experimental breakup events and for each of the 2 predicted breakup events the diameters $D_{V0.1}$, $D_{V0.5}$, $D_{V0.9}$ and D_{32} are visualized. The simulation data is plotted either with an adjusted diameter range or without any size restriction. The adjusted range takes into account the limited spatial resolution of the high speed camera ($30\,\mu\mathrm{m}$) and the maximum observed droplet diameter ($210\,\mu\mathrm{m}$). Using the adjusted

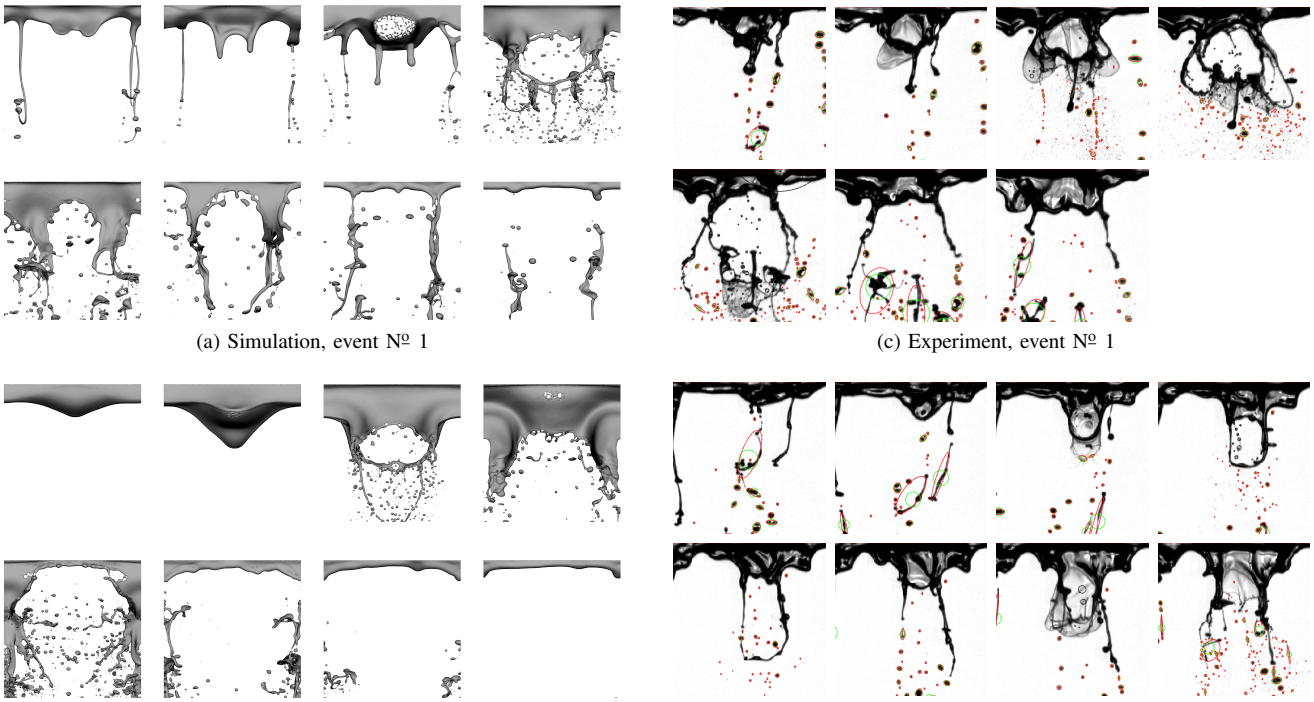

(a) Simulation, event № 1

(c) Experiment, event № 1

(b) Simulation, event № 2

(d) Experiment, event № 5

Fig. 11: Time series of different main breakup events. Numerical predictions (left) and high speed video images (right). The viewing area is $4 \times 4\,\mathrm{mm}$.

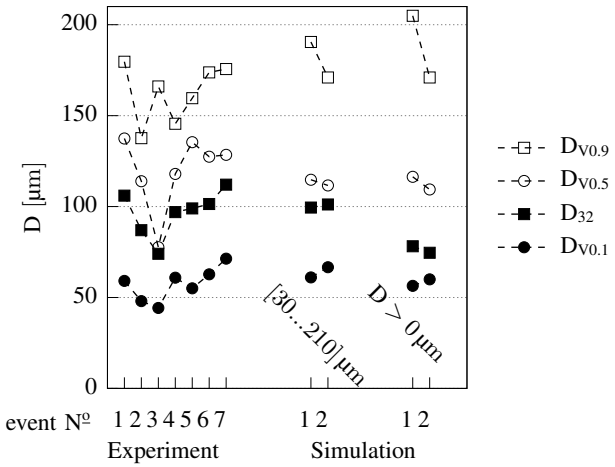

Fig. 12: Characteristic and mean droplet diameters obtained by experiment (left) and simulation. The simulation data is assessed either with an adjusted diameter range or without any size restriction.

diameter range, the predicted droplet diameters perfectly fit into the data ranges observed in the experiment. One exception is the diameter $D_{V0.9}$, which is slightly over-predicted in the first simulative breakup event. This deviation, however, can be caused by already a very few larger droplets. Furthermore, in the experimental raw data, these larger droplets can be subject to overlapping (cf. Fig. 11c) and, therefore, are not taken into account applying the visual post-processing.

Whereas the characteristic mass median diameters are not very sensitive towards the adjustment of the lower and upper droplet diameter range, the Sauter mean diameter drops by about $25\,\%$, if droplets smaller than $30\,\mu\mathrm{m}$ additionally are taken into account. Having a closer look at the high speed images, these small droplets are not missing, but their size and the low gray-scale gradient does not allow a proper contour capturing. It is, therefore, very likely, that a higher spatial resolution of the camera system would also result in a lower Sauter diameter. Table II summarizes the arithmetic mean values of the experimentally and numerically determined spray properties.

Up to now, no other numerical simulation was able to predict air-assisted atomization with an comparative degree of accuracy. By adjusting the simulative diameter range to be post-processed to the limitations of the high speed camera, the deviations of the mean spray characteristics are below or close to the measurement uncertainty.

V. Performance analysis

One of the requirements for a successful prediction of primary atomization is, that the simulation can be run within a finite period of time. An extremely high serial performance of the code and very good scalability are, therefore, indispensable. In order to compare our code to other simulation methods we introduce the unit of measure ”Iterations times Particles

TABLE II: Arithmetic mean values of droplet diameters, units are in µm.

	$D_{V0.1}$	D_{32}	$D_{V0.5}$	$D_{V0.9}$
Experiment	57	97	120	163
Simulation				
$30\,\mu m < D < 210\,\mu m$	64	100	113	181
$D > 0\,\mu m$	58	76	113	188

Per CPU-core-Second" (IPPCS). The measure describes the number of time steps, which can be performed at a given number of particles and for a given amount of computational resources.

$$\text{IPPCS} = \frac{N_{\text{particles}} \cdot N_{\text{time steps}}}{t_{\text{wall time}} \cdot N_{\text{CPU-cores}}},\ [\text{IPPCS}] = \frac{1}{\text{CPUs}}$$

An easy comparability with grid-based method is possible. Here, the number of grid cells is used. For the 3D simulation described in section II-B, on the ForHLR II cluster we achieve IPPCS-numbers of $144\,301$ at 2560 cores and $123\,053$ at $10\,000$ cores applying a Wendland kernel ($h = 1.3 \cdot dx$). This corresponds to 369 MIPPS (Million Iterations times Particles Per Second), respectively to 1251 MIPPS. In comparison to Level Set simulations with comparative flow configurations, this is at least 20 to 30 times faster [4], [11]. Warncke et al. [15] use the VoF solver `interFOAM` and achieve an IPPCS of $12\,158$ at 720 cores for an identical flow configuration like ours. Due to the coarser spatial resolution of $10\,\mu m$, the authors could admit a time step size of $50\,ns$. This is roughly 1.5 times higher than for SPH at an equal level of discretization (cf. Tab. I). However, at finer levels of discretization, the admissible time steps of (incompressible) VoF and SPH will be similar, as $\Delta t_{\text{speed of sound}} \propto h$ and $\Delta t_{\text{surface tension}} \propto h^{1.5}$. Therefore, the effect of surface tension will dominate all other time limiting conditions.

VI. Conclusion

For the first time, air-assisted atomization could be successfully predicted by means of a numerical simulation. Whereas in our recent publication [2] we were able to observe a good qualitative agreement to the corresponding experimental investigations, in this work we also demonstrated the excellent quantitative match. In contrast to state of the art grid-based methods, SPH does neither suffer from deficient mass conservation properties nor is the phase interface affected by diffusive effects. Comparing the computational speed, SPH outperforms the commonly used multiphase tools by at least one order of magnitude, if the liquid phase is subject to strong capillary forces. In this work we furthermore observed a very satisfactory convergence behavior when it comes to disintegration processes of the disperse liquid phase. The occurrence of so called single particle droplets has been found to be a helpful indicator in order to estimate the suitability of the spatial discretization.

Acknowledgment

This work was performed on the computational resource ForHLR Phase I and II funded by the Ministry of Science, Research and the Arts Baden-Württemberg and DFG ("Deutsche Forschungsgemeinschaft"). Thanks also to the guys from our super computing facility SCC ("Steinbuch Centre for Computing") for many valuable hints and for the exclusive access to the ForHLR II cluster during its trial operation.

References

[1] S. Adami, X. Y. Hu, and N. A. Adams. A new surface-tension formulation for multi-phase SPH using a reproducing divergence approximation. *Journal of Computational Physics*, 229(13):5011–5021, 2010.

[2] S. Braun, L. Wieth, T. Dauch, M. Keller, G. Chaussonnet, C. Höfler, R. Koch, and H.-J. Bauer. HPC Predictions of Primary Atomization with SPH: Challenges and Lessons Learned. *11 th International SPHERIC Workshop*, 2016.

[3] S. Braun, L. Wieth, R. Koch, and H.-J. Bauer. A framework for permeable boundary conditions in sph: Inlet, outlet, periodicity. *10 th International SPHERIC Workshop*, 2015.

[4] Olivier Desjardins, Jeremy McCaslin, Mark Owkes, and Peter Brady. Direct numerical and large-eddy simulation of primary atomization in complex geometries. *Atomization and Sprays*, 23(11), 2013.

[5] S. Gepperth, D. Guildenbecher, R. Koch, and H.-J. Bauer. Pre-filming primary atomization: Experiments and modeling. In *23rd European Conference on Liquid Atomization and Spray Systems (ILASS-Europe 2010), Brno, Czech Republic, September*, pages 6–8, 2010.

[6] S. Gepperth, R. Koch, and H.-J. Bauer. Analysis and comparison of primary droplet characteristics in the near field of a prefilming airblast atomizer. In *ASME Turbo Expo 2013: Turbine Technical Conference and Exposition*, pages V01AT04A002–V01AT04A002. American Society of Mechanical Engineers, 2013.

[7] S. Gepperth, A. Müller, R. Koch, and H.-B. Bauer. Ligament and droplet characteristics in prefilming airblast atomization. In *International Conference on Liquid Atomization and Spray Systems (ICLASS), Heidelberg, Germany*, pages 2–6, 2012.

[8] Sebastian Gepperth. *Experimentelle Untersuchung des Primärzerfalls an generischen luftgestützten Zerstäubern unter Hochdruckbedingungen*. PhD thesis, 2017.

[9] X. Y. Hu and N. A. Adams. A multi-phase SPH method for macroscopic and mesoscopic flows. *Journal of Computational Physics*, 213(2):844–861, 2006.

[10] Wolfgang E. Nagel, Dietmar Kröner, and Michael M. Resch. *High Performance Computing in Science and Engineering '16*. Springer, 2016.

[11] Madhusudan G Pai, Olivier Desjardins, and Heinz Pitsch. Detailed simulations of primary breakup of turbulent liquid jets in crossflow. *Center for Turbulence Research, Annual Research Briefs*, pages 451–466, 2008.

[12] Azriel Rosenfeld and John L. Pfaltz. Sequential operations in digital picture processing. *Journal of the ACM (JACM)*, 13(4):471–494, 1966.

[13] Henrik Rusche. *Computational fluid dynamics of dispersed two-phase flows at high phase fractions*. PhD thesis, Imperial College London (University of London), 2003.

[14] B. Sauer, A. Sadiki, and J. Janicka. Numerical analysis of the primary breakup applying the embedded dns approach to a generic prefilming airblast atomizer. *The Journal of Computational Multiphase Flows*, 6(3):179–192, 2014.

[15] K Warncke, S Gepperth, B Sauer, A Sadiki, J Janicka, R Koch, and H-J Bauer. Experimental and numerical investigation of the primary breakup of an airblasted liquid sheet. *International Journal of Multiphase Flow*, 91:208–224, 2017.

[16] L. Wieth, S. Braun, R. Koch, and H.-J. Bauer. Modeling of liquid-wall interaction using the Smoothed Particle Hydrodynamics (SPH) method. In *26th European Conference on Liquid Atomization and Spray Systems (ILASS-Europe 2014), Bremen*, 2014.